Nano Energy 120 (2024) 109134

Contents lists available at ScienceDirect

Nano Energy

journal homepage: www.elsevier.com/locate/nanoen

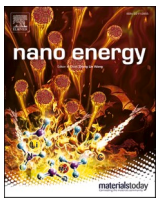

Thermal insulating textile based triboelectric nanogenerator for outdoor wearable sensing and interaction☆

Haishuang Jiao [a,b,1], Xiangde Lin [c,1], Yao Xiong [b,1], Jing Han [b], Yang Liu [a,b], Jiahong Yang [a,b], Shishuo Wu [a,b], Tao Jiang [a,b], Zhong Lin Wang [d,*], Qijun Sun [a,b,e,**]

[a] Center on Nanoenergy Research, School of Chemistry and Chemical Engineering, Guangxi University, Nanning 530004, PR China
[b] Beijing Institute of Nanoenergy and Nanosystems, Chinese Academy of Sciences, Beijing 101400, PR China
[c] School of Medical Instrument, Shanghai University of Medicine & Health Sciences, Shanghai 201318, PR China
[d] Georgia Institute of Technology, Atlanta, GA 30332-0245, United States
[e] Shandong Zhongke Naneng Energy Technology Co., Ltd., Dongying 257061, PR China

ARTICLE INFO

Keywords:
Textile TENG
Thermal insulating textile
Energy harvesting
Outdoor wearable sensing
Wearable interactive interface

ABSTRACT

People have shown increasing interests in outdoor activities in recent years. However, the development of smart outdoor clothing for sophisticated health monitoring and multifunctional interaction remains challenging. Here, we develop a thermal-insulating textile (TI-textile) based TENG (TI-TENG) composed of multiple functional layers, including the crucial triboelectrification layer, Ag-coated Nylon electrodes, windproof outer textile, and inner textile lining. The triboelectric output properties of the TI-TENG can be enhanced by material modification and structural optimization. The prepared TI-TENG is demonstrated with multifunctionality (e.g., thermal insulation and antibacterial properties) and intelligences (e.g., sensing and energy harvesting function). In addition, an intelligent human motion monitoring as well as an outdoor wireless signal transmission system are developed by employing the TI-TENGs as self-powered wearable sensors and human-machine interactive interfaces, which are ready for one-button call for emergency rescue during the outdoor activities. The available large-scale production of TI-textile also promise TENG with great commercial potentials, offering a new research direction for multifunctional wearable devices toward self-powered sensing, energy harvesting, and human-machine interaction.

1. Introduction

Outdoor activity is essential for human health and brings many physical and mental benefits to humans [1]. Assimilating into the natural environments with physical/mental healing power during outdoor activities can effectively help to alleviate the appearance of health problems. Generally, outdoor enthusiasts need to be aware of various weather issues (e.g., snow, rain, and wind) during long-term hiking or other physical activities. Extreme weather conditions may easily lead to physical discomfort, loss of temperature, and even loss of connection [2]. Accordingly, it is important to enhance the functionality of outdoor wearables (e.g., thermal/cold insulation, moisture penetrability, quick-drying, antibacterial properties) with facile communication systems, especially with energy supply function. As most of the electronic wearables are powered by conventional batteries, they are not sustainable and inconvenient to be recharged/maintained in outdoors. It is very important to develop outdoor wearables with self-powered sensors to address the issues of non-sustainability and potential environmental pollution from wasted batteries [3]. In the era of Internet of Things, triboelectric nanogenerator (TENG), which can convert random, disordered and low-frequency surrounding mechanical energy into electrical energy, is considered highly promising to solve the energy-supply

☆ Prof Zhong Lin Wang, an author on this paper, is the Editor-in-Chief of Nano Energy, but he had no involvement in the peer review process used to assess this work submitted to Nano Energy. This paper was assessed, and the corresponding peer review managed by Professor Chenguo Hu, also an Associate Editor in Nano Energy.

* Corresponding author.
** Corresponding author at: Center on Nanoenergy Research, School of Chemistry and Chemical Engineering, Guangxi University, Nanning 530004, PR China.
E-mail addresses: zhong.wang@mse.gatech.edu (Z.L. Wang), sunqijun@binn.cas.cn (Q. Sun).
[1] These authors contributed equally to this work.

https://doi.org/10.1016/j.nanoen.2023.109134
Received 15 September 2023; Received in revised form 10 November 2023; Accepted 23 November 2023
Available online 29 November 2023

problems in some extreme situations or environments [4,5]. Assisted with TENGs, self-powered outdoor wearable monitoring systems can be implemented and readily utilized [1,6–10], which are quite necessary for the outdoor enthusiasts to engage in long-term hiking or physical activities.

In past few years, scientists have been deploying great efforts in improving TENG output performance to power commercial electronic devices, but it is still a severe challenge to achieve high output currents. Several approaches are commonly utilized to improve the conversion efficiency of TENG: including the elaborate selection of triboelectric materials with distinct polarity difference according to the triboelectric sequence [11], modulation on the surface permittivity, and increasing the effective contact area or surface roughness via physical/chemical/micropatterning methods. In term of the selection on triboelectric materials, the capability of attracting electrons is of great importance to improve the electrical properties of TENG [12,13].

The commonly used positive triboelectric materials in the triboelectric series are metals (Al, Au), polyamides (PA), common oxide materials (ZnO, NiO) or textiles (Nylon, polyester) [14–18], while the negative triboelectric materials are mostly electronegative polymers, such as fluorinated ethylene propylene (FEP), polytetrafluoroethylene (PTFE), and polydimethylsiloxane (PDMS) [19–22]. Because of the high polarity and processability, FEP is an excellent candidate for the negative triboelectric material in TENGs [21,23,24]. In contrast, textile based positive triboelectric material is readily engineered with porous, hierarchical or other sophisticated micro/nano structures to increase the effective contact area and construct flexible TENGs [25–27]. Among the reported wearable TENGs, textile TENGs can be readily used for human motion monitoring and power supply, attracting more and more attentions due to their flexibility, suitability, breathability, affordability, and scalable production [28–40]. Textile TENGs have been developed for various applications based on sophisticated structures and diverse materials, e.g., coverall, rescue clothing, fire-protection suit and outdoor clothing. As is known, the outdoor clothes can protect human against the bleak wind, but their weight and thickness commonly lead to uncomfortableness for long-time outdoor activities. Accordingly, it is important to decrease the heaviness/thickness of the functional outdoor clothes but meanwhile improve the thermal insulation performance. Until now, there is still a lack of research on the functional outdoor clothes concerning this point, especially the smart outdoor clothes combined with textile TENGs embodying with energy-harvesting capacity and interactive applications.

In this study, we develop a thermal-insulating textile (TI-textile) based TENG (TI-TENG) composed of multiple functional layers, including the core FEP/TI-textile as the triboelectrification layer, Ag-coated Nylon electrodes, windproof textile as the protective outer layer, and textile lining as the inner layer. The core TI-textile is elaborately characterized and further optimized with material modification and structural design to enhance the triboelectric output properties of the TI-TENG. Based on the hierarchical structure of the core TI-textile, the prepared TI-TENG is endowed with multifunctionality (e.g., thermal insulation and antibacterial properties) and intelligences (e.g., energy-harvesting and sensing function). Furthermore, the TI-TENG has various bending capabilities and exhibits stretching properties in all directions, allowing the bending and recovery of the joints. A multifunctional and intelligent human health motion monitoring as well as an outdoor wireless signal transmission system are developed by employing the TI-TENGs as self-powered wearable sensors and human-machine interactive interfaces, through which health and motion monitoring can be achieved through joint flexion. It is also possible to realize the function of one-button call for rescue during the outdoor activities in case of emergency. The developed TI-textile based TENG is highly adjustable to satisfy the diversity of functions, complexity of human motion monitoring and variations of external environment, which also brings high-level comfort and satisfaction to the human body during daily wearing [41–44].

2. Results and discussion

In outdoors activities, people have been pursing "independent of the environment" and "long-lasting" energy-harvesting wearable technology to power portable electronic devices or recharge batteries. It is even of great significance to save people's life in time in emergency situations by integrating wireless communication systems and health monitoring functions. Nowadays, various wearable energy-harvesting technologies have been intensively investigated which can coordinate and complement with each other, but there are still many shortcomings. For example, during the exploration in the forest, the application of thermoelectric generators or solar cells may be restricted due to the lack of heat source and sunlight. Conventional electromagnetic generators with large size and high-frequency requirement also conflict against wearability (or portability). Recently emerging TENG technology, which can capture low frequency mechanical energy, is still lack of investigation for outdoor activities. Noting that the waterproof, breathability, heat-insulation, and lightweight is the necessity and basic requirement for people who encounter extreme rain, wind, and snow during wilderness exploration, the development of textile-based TI-TENG can further deliver extraordinary energy-harvesting, healthcare, smart sensing, and interactive functions. As shown in Fig. 1**a**, the proposed multi-functional TI-TENG consists of the outer protective windproof/waterproof textile, the inner textile lining, and the core FEP/TI-textile, which can be placed at specific/required position on human body and convert biomechanical energy into electrical energy for powering portable electronic devices, monitoring health in real time and driving a wireless transmitter for sending distress signals.

Multilayer textile stacking is beneficial to improve thermal insulating properties in extremely cold weather and does not increase the burden of the wearer. Accordingly, we select the versatile TI-textile and packaged with the outer protective windproof/waterproof textile and the inner textile lining (Fig. 1**b**). The hierarchically structured TI-textile is different from conventional thermal insulating cloth and has superior lightweight properties (Fig. S1a); polyester microspheres as the main modification material on the underlying textile (Figs. 1**c** and 1**d**) lead to the larger contact area; it also has outstanding moisture permeability after chemical modification (a 2 μL droplet can be completely absorbed into the TI-textile within 1 s, Fig. 1**e**, Movie S1; the contact angle before modification is ~125°, Fig. S1b), which is useful for the sensor to monitor body health by monitoring the ionic concentration of sweat; in addition, it has feasible scalability (Fig. 1**f**), good breathability (Fig. S1c-**d**) [45,46], excellent flexibility (Fig. S1e), and quick-drying properties (Fig. S1f). The thermal insulation TI-TENG evaluated by YG461E air permeability tester shows permeability of 6.02 $mm \cdot s^{-1}$, which is still comparable to conventional insulating textiles according to GB_T5453:1997. Accordingly, the TI-textile has not only superior lightweight, but it also shows better thermal insulating properties with versatility than conventional insulating cloth.

Supplementary material related to this article can be found online at doi:10.1016/j.nanoen.2023.109134.

Its thermal insulating properties are further explored by incorporating TI-textile with a custom hot plate, as shown in Fig. S2. The hot plate and an aluminum sheet are used to simulate the temperature variation by the thermal radiation. The samples are placed on the custom facility and the temperature difference ΔT ($\Delta T = T_{\text{hot-plate}} - T_{\text{textile}}$ (°C)) between the textile surface and the custom hot plate is measured using a digital thermometer (UT-325). The temperature difference ΔT is directly related to the thermal insulating properties (larger ΔT means better thermal insulation). We try to compare the thermal insulating properties of the TI-textile, polyester cloth, and polyester blended cotton cloth by extracting the target temperature after putting them on the hot plate in different temperatures (45 °C, 54 °C, 65 °C, and 75 °C, Fig. S3). Fig. 1**g** clearly exhibits the TI-textile has the lowest temperature difference on the hot plate at 65 ℃ [45–47]; Table S1 further manifests that the temperature difference ΔT of the TI-textile is

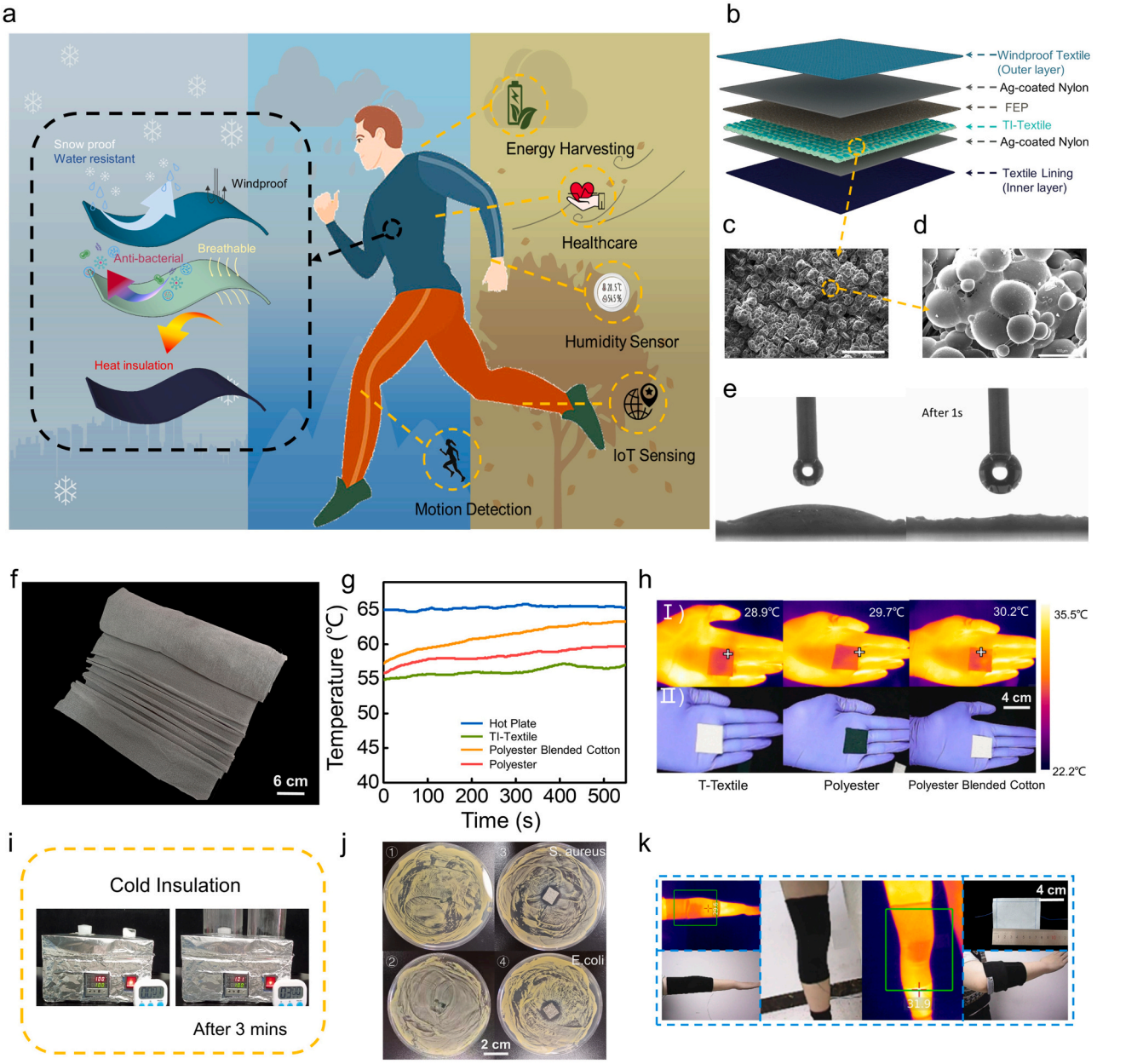

Fig. 1. Application scenarios, structures, and properties of the TI-TENG. (a) Application scenarios and composition of thermal insulating clothes. (b) Schematic demonstration of the TI-TENG. (c, d) SEM images of the TI-textile in plane. Scale bar: 1 mm and 100 μm, respectively. (e) DI water drops before and after falling on TI-textile surface. (f) Photographs of the TI-textile. (g) The surface temperatures of the various samples maintained on an open-air hot plate at 65 °C. (h) I) Infrared camera thermal image of different samples in the palm; II) photo images of the samples. (i) Photograph of the cold insulating properties of TI-textile. (j) Antibacterial performance of TI-textile against S. aureus and E. coli cultivation. (① and ② colonies cultivation under polyester, ③ and ④ colonies cultivation under TI-textile). (k) Photograph of wearing the thermal insulating strap.

higher than the other two samples; both of the results represent TI-textile has the best thermal-insulating properties among the control samples. The different thermal insulating properties of the three sampls can also be visually observed according to the thermographic imaging (TI-textile shows the lowest temperature of 28.9 ℃, Fig. 1**h**). Cold insulating properties of the TI-textile are also characterized as demonstrated in Fig. 1**i**, Fig. S4, and Movie S2, in which two ice cubes are placed on the surface of the TI-textile and tinfoil, respectively, and the ice melting rate is recorded. By setting the hot plate at 100 °C, the ice on the TI-textile surface melts significantly slower than that on the tinfoil. The above results indicate that TI-textile has excellent thermal insulating properties due to its low thermal conductivity calculated by the Guarded hot plate apparatus method (a standard method to evaluate thermal conductivity, Table S2). Besides, the TI-textile has excellent antibacterial potential in relation to Escherichia coli (E. coli) and Staphylococcus aureus (S. aureus). As shown in Fig. 1**j**, we can observe that the distribution of E. coli and S. aureus is inhibited in the area where TI-textile is placed [48]. Notably, the hierarchical structure in the TI-textile also promises with higher triboelectric output properties without compromising the wearable comfort. Compared with smooth polyester surface (Fig. S5a, S5b), the modified polyester microspheres on the TI-textile (Fig. 1**c**) offer more active sites and larger surface areas for charge transfer during the triboelectrification process (Fig. S5c-**e**) [49]. Based on the advantages of both thermal insulation and high triboelectric output, the TI-textile based TENG can be readily packaged in dressing belt and worn on human body where the thermal insulation

and health/motion monitoring is required (e.g., wearing on the knees, elbows, and other joints, Fig. 1**k**).

Supplementary material related to this article can be found online at doi:10.1016/j.nanoen.2023.109134.

To measure the output performance of the TENG based on TI-textile, we have tried to construct four types of TENG devices in different structures (both in contact-separation mode) and choose the device with the best performances. The first type is the basic TI-TENG, which is composed of Ag-coated Nylon/TI-textile/FEP/Ag-coated Nylon as shown in Fig. 2**a**. The second type is a packaged TI-TENG to satisfy the outdoor wearable applications, which is composed of the basic TI-TENG packaged by the outer water/windproof textile and inner lining cloth as shown in Fig. 2**d**. The other two types of devices are shown in Fig. S6a and S6c, in which the Ag-coated Nylon electrodes are completely replaced by Ag tape. Figs. 2**b** and 2**d** show the working principles of the TI-TENG and the packaged TI-TENG, respectively, assisted with the charge transfer process according to the triboelectrification and electrostatic induction. We take the TI-TENG as the example (with Ag-coated Nylon as electrodes, in contact-separation mode) to explain the working principle. When the TI-textile contacts with the FEP layer with strong polarity, opposite surface electrostatic charges will be induced at the contact interface because of the contact-electrification effect (Fig. 2**b (I)**). Electrons transfer from the surface of the TI-textile to the FEP surface in higher polarity (FEP surface is negatively charged). The surface of TI-textile will have the same amount of positive charges, and there is no electrical potential difference between them at this state. When the FEP and the TI-textile surfaces gradually separate, the electrical potential difference will be produced between the two layers in the open-circuit circumstance (Fig. 2**b (II)**). When the TI-textile and FEP fully separate, the electrical potential difference reaches the maximum value (Fig. 2**b (iii)**). When the TI-textile moves back toward the FEP layer, the electrical potential between them will gradually decrease to the previous level (Fig. 2**b (IV)**). When the TI-textile and FEP fully contact with each other again, the device returns to its initial electrostatic equilibrium state (Fig. 2**b(I)**). Similar working principle for the packaged TI-TENG is presented in Fig. 2**e**. The output performances of all the four different TENGs (open circuit voltage (V_{OC}), short circuit current (I_{SC}), and transferred charge (Q_{SC})) are evaluated by Keithley 6514 upon contact-separation motions driven by a digital-controlled linear-motor. When the contact-separation frequency increases from 1 to 5 Hz (separation distance = 50 mm and contact area = 3 cm × 3 cm), the I_{SC} of the TI-TENG with Ag-coated Nylon electrode increases from 1.15 to 9.31 μA, and the V_{OC} and Q_{SC} remain essentially the same (87.98 V, 51.32 nC, respectively, in Fig. 2**c**). Under the same condition, the TI-TENG with Ag-tape electrode is 157.15 V, 59.64 nC (Fig. S6b). The V_{OC} and Q_{SC} of the packaged TI-TENG with Ag-coated Nylon electrode are 138.04 V and 51.36 nC (Fig. 2**f**), while the triboelectric outputs for the packaged TI-TENG with Ag-tape electrode are 146.87 V and 56.37 nC, respectively (Fig. S6d). The typical TENG output variation related to the frequency can be explained as follows. According to the Gauss theorem [50,51], the voltage between the two electrodes can be given by

$$V = -\frac{Q}{S\varepsilon_0}(d_0 + x(t)) + \frac{\sigma x(t)}{\varepsilon_0}$$

This is the basic equation for the contact-separation mode TENG and can be utilized to calculate its output properties. First, two special cases of the open-circuit (OC) condition and short-circuit (SC) condition are

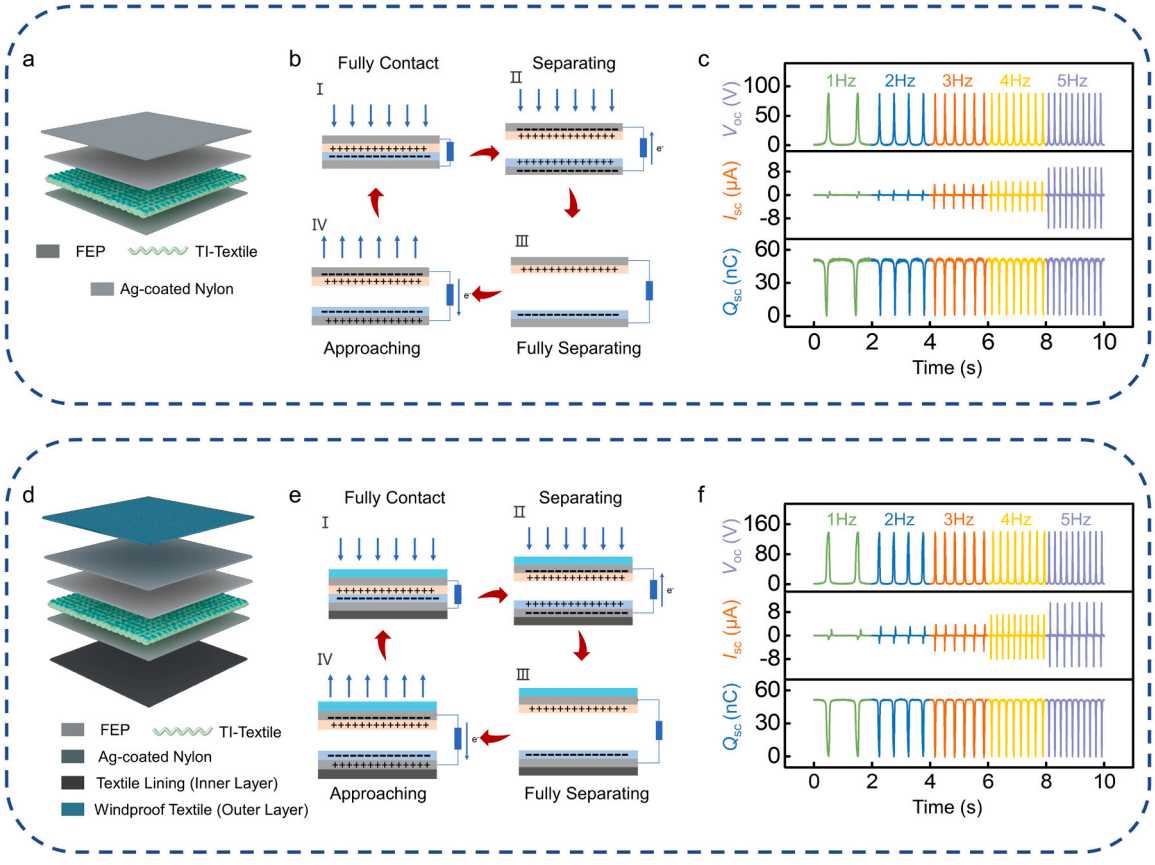

Fig. 2. Working mechanism and electrical performance of TI-TENG. Diagram of the multi-layer TENG structure: (a) the basic TI-TENG structure and (d) the TI-TENG packaged with windproof textile and textile lining. Schematic diagram of the working principle of the multi-layer vertical contact-separation mode: (b) the basic structure TI-TENG and (e) the TI-TENG packaged with windproof textile and textile lining. (c) I_{SC}, V_{OC}, and Q_{SC} of the basic structure TI-TENG and the TI-TENG packaged with windproof textile and textile lining under different contact frequencies (1–5 Hz).

analyzed. At OC condition, there is no charge transfer, which means that Q is 0. Therefore, the open-circuit voltage V_{OC} is given by

$$V_{OC} = \frac{\sigma x(t)}{\varepsilon_0}$$

At SC condition, V is 0. Therefore, the transferred charges are

$$Q_{SC} = \frac{S\sigma x(t)}{d_0 + x(t)}$$

In these equations, ε_0 is permittivity of vacuum, x is the separation distance between the two triboelectric charged layers, and S is the electrode area. The voltage is the function of $x(t)$ and the static charge density of σ, which shows no response to the frequency. The transferred charges are the functions of $x(t)$, the electrode area of S, and the static charge density of σ, which also show no response to the frequency.

$$I_{SC} = \frac{dQ_{sc}}{dt} = \frac{S\sigma d_0}{(d_0 + x(t))^2}\frac{dx}{dt} = \frac{S\sigma d_0 v(t)}{(d_0 + x(t))^2}$$

This equation means that the displacement current density (which also determines the output current) is proportional to the speed at which the two dielectrics contact/separate. The electrical potential distributions of the TI-textile based TENG with four different structures in contact-separation mode are also simulated by employing COMSOL Multiphysics software as illustrated in Fig. S7a-**d**. The TI-TENG with Ag-tape electrode shows the highest output properties. In addition to the device structure, previous studies have shown that the environmental humidity has a significant effect on the output properties of TENG. In general, high humidity significantly reduces the triboelectric output of the TENG device. The decrement trend can be assigned to several reasons induced by increased humidity, including poorer charge accumulation, increased contact resistance, reduced electron transfer process, etc. In this study, a humidifier is used to produce vapor in the confined environment to simulate different ambient humidity levels and a wireless hygrometer is used to monitor the real-time humidity. The output voltages of the TI-TENG are tested at 11 different levels of relative humidity (RH, Fig. S8a). As the ambient humidity increases, the output voltage of the TI-TENG exhibits a decreasing tendency and reaches a saturate level with the RH at ~78 % (Fig. S8b) [52,53]. When the adopted TI-TENG adds the inner and outer protective textile, the RH effect on the triboelectric output can be effectively alleviated. Besides, the packaged TENG device with Ag-tape electrode can further prevent the humidity influence on the output compared with the Ag-coated Nylon electrode. Accordingly, we choose the TI-TENG with Ag-tape electrode for the following applications (also with the highest output performance). Long-term stability of the TI-TENG is also investigated as shown in Fig. S8c, in which the V_{OC} and Q_{SC} of the TI-TENG exhibit no significant degradation during 300-day intermittent testing. The result indicates the excellent durability and stability of our TI-TENG for long-term daily use. For the sensing TI-TENG in single electrode mode, the working mechanism is shown in Fig. S9a, which is similar to the contact-separation mode. The only difference is that the electron transfer occurs between the two Ag electrodes in contact-separation mode, while it occurs between the Ag electrode and the ground in single electrode mode. The electrical performances (I_{SC}, V_{OC}, and Q_{SC}) of the single electrode mode TI-TENG are also evaluated, which indicate similar variation trends with the contact-separation mode under different operation frequencies (Fig. S9b). However, the electrical performance is lower (at 5 Hz, I_{SC} = 1.81 μA, V_{OC} = 66.98 V, and Q_{SC} = 23.35 nC) due to the finite contact area of the textile structure. The single electrode mode TI-TENG with relatively lower output can be used for a tactile sensor (which will be discussed later).

The washability, durability, stretchability, and thermal insulating properties affect the comfort of flexible and wearable sensors. Washability is significant for smart textiles in practical applications. In this regard, the triboelectric output of the TI-TENG is explored after washing in water for 2, 4, 6, 8, and 10 h, respectively. As presented in Fig. 3**a-c**, the TI-TENG shows relatively constant outputs without significant changes after 10 h washing. As the durability is a critical parameter to flexible and wearable sensors, we further discuss the stability of the TI-TENG after thousands of contact-separation cycles at a frequency of 3 Hz. The V_{OC}, output power, and Q_{SC} of the TI-TENG is found to remain stable after 8000 cycles (Fig. 3**d-f**) [54]. Mechanical properties of the TI-textile in different directions are also investigated by means of stress vs. strain curves (Fig. 3**g**). The fracture strain of the TI-textile is ~48 % in the diagonal direction and the fracture stress is ~7.74 MPa, which is several times higher than the stress in the other two directions (weft and warp directions). In addition, the output stability of the TI-TENG during stretching is also important. The output performance of the TI-TENG in the diagonal direction is tested under different tensile conditions. Corresponding electrical output of Q_{SC}, V_{OC}, and I_{SC} for the TI-TENG at various tensile strains (under the same force) are shown in Figs. 3**h**, 3**i**, and **S10**, respectively. The output properties increase as a function of the stretching ratio, which is probably related to the closer contact between TI-textile and FEP during stretching and the resultant increment of effective contact area. Moreover, Fig. 3**j** displays the electrical outputs (V_{OC}, I_{SC}, Q_{SC}) of the packaged TENGs with 1, 2, 3, 4, and 5 layers of TI-textile. The results indicate that the output tends to be saturated when the layer number of TI-textile reaches three layers. To further examine the thermal insulating performance of the TI-TENG with multiple layers of TI-textiles, we also conduct the relevant experiments as discussed above. The prepared samples with different numbers of layers (from 1 to 5) are placed on the hot plate (45 °C) and their temperature variations are monitored in real time by using a digital thermometer (Fig. 3**k**). The temperature drops between the hot plate and the sample under examination are directly proportional to the thermal insulating performance. The temperature differences ΔT for the TI-TENGs with 1, 2, 3, 4, and 5 layers of TI-textile are 4.8 °C, 5.6 °C, 7.6 °C, 8.1 °C, and 9.4 °C, respectively. Furthermore, the hot plate temperature is set to be 65 °C (Fig. 3**l**), 54 °C (Fig. S11a), and 75 °C (Fig. S11b) to check the thermal insulation properties of TI-textile in different layers. The same temperature decrement tendency is observed for all the five kinds of TENG samples (Table S3). The thermal images of the five samples are also placed on the palm to vividly demonstrate the thermal insulating properties of the TI-TENG (Fig. S12). After thermal equilibrium, the average temperatures for the TI-TENGs with 1, 2, 3, 4, and 5 layers of TI-textile are 29.4 °C, 29.3 °C, 28.9 °C, 28.0 °C, and 27.8 °C, respectively. More embedded TI-textile layers can improve the thermal insulation capacity.

As is known, human sweat is one of the most frequently utilized and significant biosensing indicators for human health surveillance. In daily life, our clothes can absorb the sweat during continuous outdoor activities and enable us to exercise comfortably for a long period of time. Regarding to this concern, the TI-textile with excellent air permeability is also investigated as a wearable sweat sensor. The sweat absorption process is simulated by wearing the TI-textile on the skin assisted with a belt, which is divided into four steps: wetting, absorption, spreading, and evaporation (Fig. 4**a**). During long-time outdoor activities, human body is prone to perspiration and will gradually wet the TI-textile. Due to the hydrophilic groups on the surface of the TI-textile, the perspiration wets the TI-textile and the sweat is adsorbed on the inner attached surface. Then, the continuous perspiration spreads over the TI-textile and gradually expands the sweat-absorption area. Finally, the absorbed sweat will evaporate outward to achieve a quick drying effect. After evaporation of perspiration, corresponding energy dispersive X-ray spectroscopy (EDS) elemental mappings of TI-textile surface are exhibited in Fig. 4**b**. It indicates that when the concentration of NaCl solution changes, the surface charge of the TI-textile (after drying) will also change and lead to different triboelectrification properties (i.e., different triboelectric outputs) during the contact-separation process in TI-textile based TENG sweat sensor.

To evaluate the sensing capability of the TI-TENG as a sweat sensor,

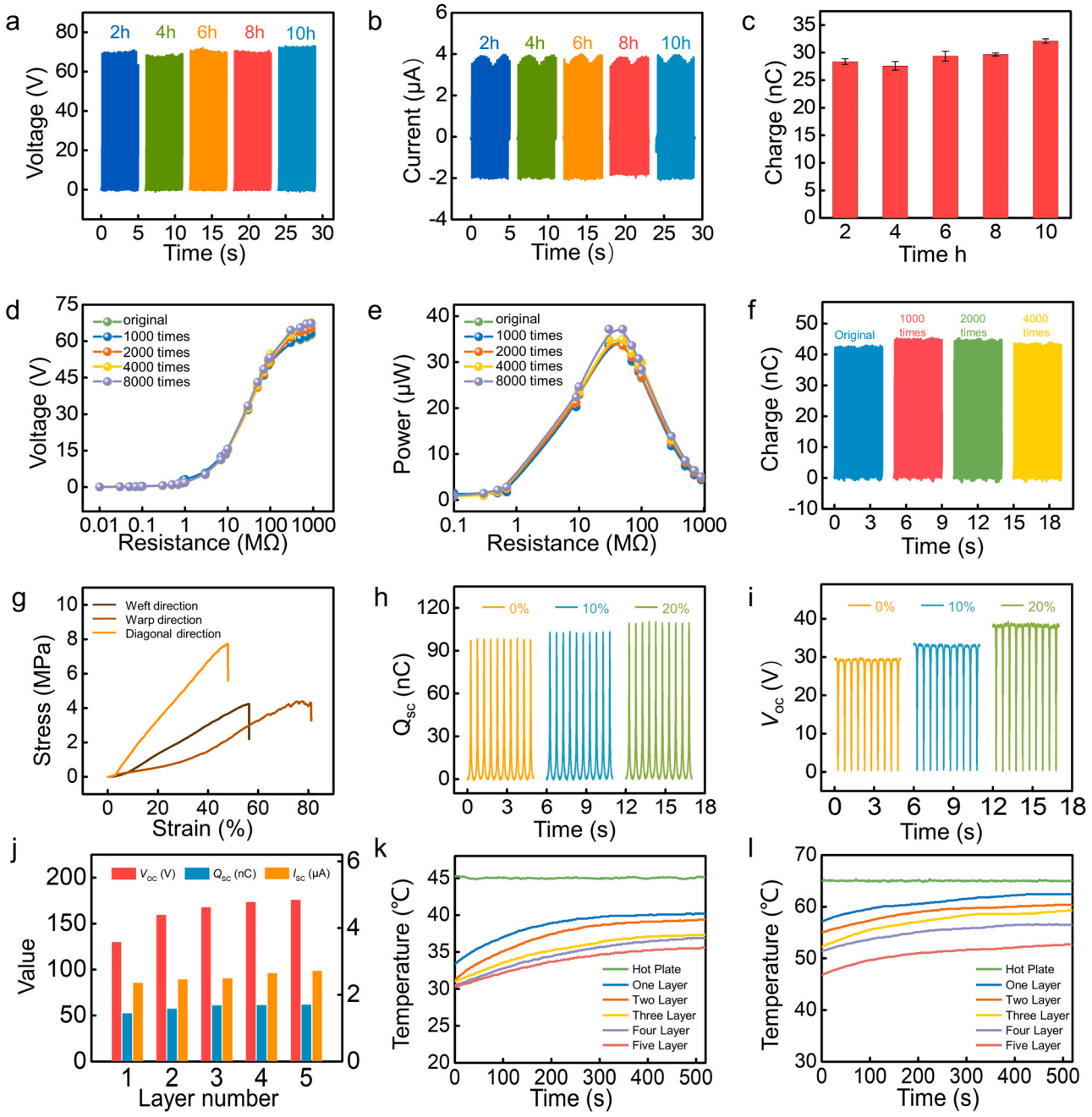

Fig. 3. Washability, long-term stability, stretchability, and multi-layer performances of the TI-TENG. The washing properties of the TI-TENG for long time: (a) open-circuit voltage, (b) short-circuit current, and (c) transferred charges. Comparison of (d) voltage, (e) power and (f) current for the TI-TENG with different friction times (original, 1000 times, 2000 times, and 4000 times). (g) Stress-strain curves of the TI-textile in various directions. Output properties at different tensile conditions (contact-separation frequency of 2 Hz): (h) transferred charge and (i) open-circuit voltage. (j) I_{SC}, V_{OC}, and Q_{SC} of the TI-TENG composed of multi-layer TI-textile at the contact-separation frequency of 1 Hz. Surface temperatures of various layers of TI-textile at (k) 45 °C and (l) 65 °C on an open-air hot plate.

the sensing signal V_{OC} (Fig. 4**c**) and the transferred charge Q_{SC} (Fig. S13b) are recorded under contact-separation between the FEP and TI-textile (after drying with NaCl solution in different concentrations). The amount of charge transferred between the surfaces of the materials depends on the relative polarity between the two materials in contact. According to Gauss's theorem [51,55], it is stated that the factors affecting Q_{SC} are $x(t)$ (the separation distance between the two triboelectric charged layers), S (the electrode area), and σ (the static charge density). The experimental results show that the amount of transferred charge decreases with increasing NaCl concentration when $x(t)$ and S remain constant. As mentioned in previous reports [56,57], electrolyte concentration is negatively correlated with the charge of the electrolyte droplet. The concentration has a large effect on the surface charge, where the ionization of the surface groups creates an interfacial charge, and variation of the surface charge causes a change in polarity. With increasing NaCl concentration, V_{OC} and Q_{SC} exhibit gradual decrement tendency as well. More specifically, the V_{OC} peak value for the TI-TENG with the TI-textile immersed in 0.7 mol/L NaCl (test after drying) is 67.5 % of that for the TI-textile immersed in DI water, and the Q_{SC} is 83.1 % of that for the TI-textile immersed in DI water. When the ion concentration is below 0.01 mol/L, the output voltage shows a significant decrement tendency (meaning a better sensitivity); when the ion concentration is above 0.01 mol/L, it shows a slight decrement tendency (presenting a poorer sensitivity). As demonstrated in Fig. 4**d**, the output voltages

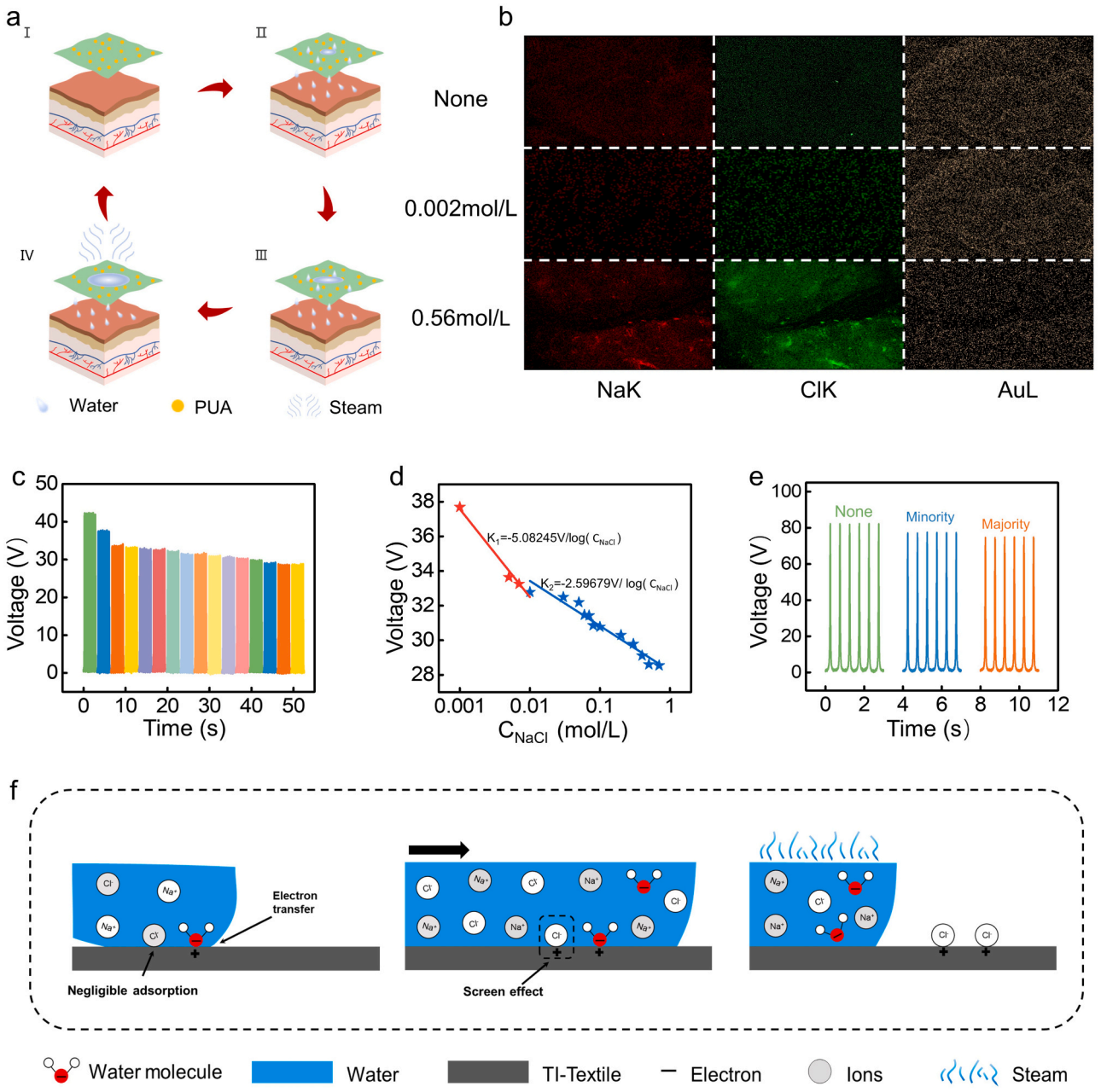

Fig. 4. Sweat sensors for physiological health monitoring. (a) The process of absorbing sweat by TI-textile. (b) EDS mapping of the dried TI-textile immersed in various concentrations of NaCl solutions with a scale bar of 100 μm. (c) Dynamic transient voltage response in response to increasing concentration. (d) Open-circuit voltage generated with the dried TI-textile immersed in DI water and various concentrations of NaCl solutions (0.001–1 mol/L). (e) Real-time monitoring on the dried TI-textile which is immersed in minority and majority amount of sweat. (f) Schematic diagram of dynamic process on the surface of TI-textile immersed in NaCl solution.

exhibit a linear decreasing trend fitted with a simple logarithmic function ($y = K_1$ log $(x) + A$). The slopes of the fitting curves (K, i.e., the sweat sensitivity) are calculated as $K_1 = -5.08245$ V/log(M) and $K_2 = -2.59679$ V/log(M). Regarding the normalized sensitivity ($(V_0\text{-}V)/V_0$), it increases by 12 %/decade and 6 %/decade, respectively (Fig. S13a, both are in good linearity). The recorded Q_{SC} vs. C_{NaCl}, also shows two-stage linear relationships with the slopes of the fitting curves at −1.98792 V/log(M) and −0.9818 V/log(M), respectively (Fig. S13c). The normalized sensitivities ($(Q_0\text{-}Q)/Q_0$) are 13 %/decade and 7 %/decade, respectively (Fig. S13d), both of which also show good linearity. This result is consistent with previous report that a saturated NaCl solution leads to a 40 % decrement in the triboelectric charge density [58]. The achieved sensitivity of the TI-TENG is also comparable to that of commercially available salinity sensors. As shown in Fig. 4**e**, we have also tested the real-time V_{OC} of the TI-textile after it has been wetted by sweat and dried at different sweat amounts during outdoor activities. As shown in Fig. S13e and S13f, there is almost no charge transfer for the TI-TENG under sweated state. This result also indicates that no additional liquid-solid dynamic contact process is established at the interface between the TI-textile and NaCl solution (main component of sweat).

As the ion concentration reaches a specific threshold, different kinds of ions will have distinguishing influences on the amount of charge transfer between the liquid and the solid. Fig. 4**f** shows a schematic illustration of the process for charge transfer between the NaCl solution and the TI-textile. When the NaCl solution in higher concentration

comes into contact with TI-textile, electron transfer and negligible adsorption take place at the contact interface of the two materials. When the liquid starts to flow through the textile, the Na^+ takes the place of the positively charged water molecules (H_3O^+) in the solution, and negligible adsorption and shielding effects prevent the following electron transfer between the TI-textile and water molecules [59]. When the solution evaporates and separates from the surface of the TI-textile, the majority of the ions on the surface of the TI-textile moves off with the liquid and only a minority of the Cl- ions is left behind and attracted to the surface of the positively charged TI-textile due to the electrostatic attraction. As shown in Table S4, when the NaCl concentration increases, the amount of free Na^+ and Cl^- increases, leading to an increment in the percentage of Cl^- adsorbed on the TI-textile surface due to electrostatic adsorption.

Since the TI-textile based TENG shows high output properties, it can easily be adapted to work as a power source. To power portable commercial electronics, the output of TENG is generally first stored in energy storage elements (e.g., batteries or capacitors) and then used for further energy supply (circuit diagram in Fig. S14a). The self-powered energy supplier is prepared by integrating the TI-TENG with a capacitor to power the series-connected electronics, including the component of TI-TENG, bridge rectifier, and capacitor as AC power source, AC to DC converter, and energy storage part, respectively. Fig. S14b shows the charging curves of the TI-TENG (3 cm × 3 cm) for different capacitors of 1, 2.2, 3.3, 4.7, and 10 μF, which takes 6, 18, 23, 70, and 450 s to charge the capacitors to 3.3 V, respectively. After charging a 4.7 μF capacitor to 20 V in 39 s, the TI-TENG based energy supplier is capable to uninterruptedly power nine LEDs for repeatable usage (Fig. S14c). The effective output power of the TI-TENG is also investigated through the connection of various loads. As shown in Fig. S14d, the output voltage according to the external load resistance tends to increase because of Ohm's law. At an external load of 50 MΩ, the output power can reach a maximum value of 34.78 μW (for the contact area of 3 cm × 3 cm, the maximum instantaneous power density reaches 38.64 mW/m^2, Fig. S14d), and a maximum average output power density of 1.87 mW/m^2 (Fig. S14e). As the output consistency of the TI-TENG plays an essential role in ensuring

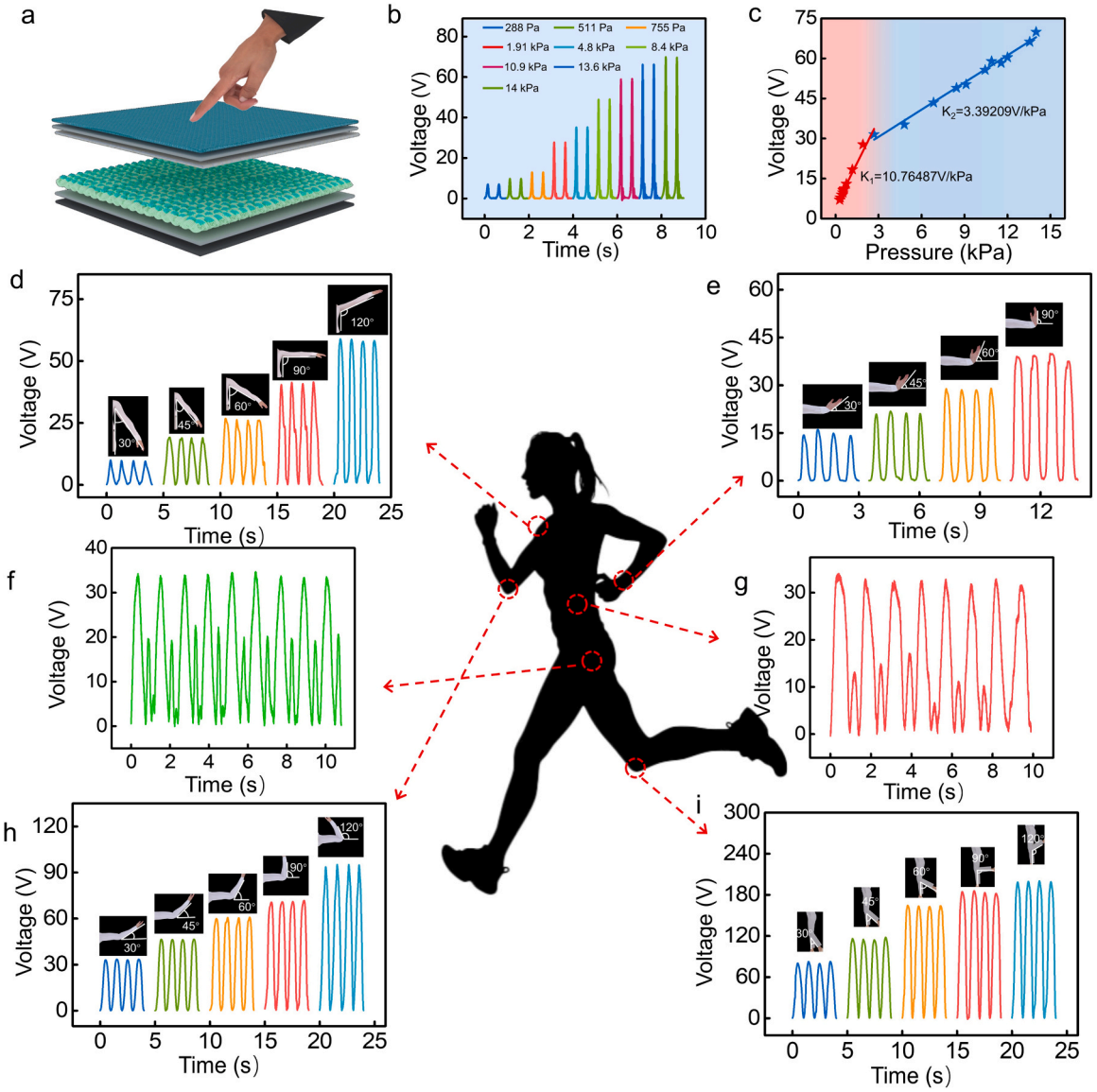

Fig. 5. Monitoring of human physiological signals. (a) Schematic demonstration of the pressure sensor. (b) The outputs of the TI-TENG under various pressures. (c) The outputs of the TI-TENG as a function of loading pressure variations. (d) Real-time monitoring of the bending angles of the arm by the TI-TENG. The insets exhibit different states of motion. (e) Output signals in response to wrist bending at 30°, 45°, 60°, and 90°. (f) Output signals of the TI-TENG taken at the hip when the tester raises his leg. (g) Voltage response to waist movements measured by mounting the TI-TENG on the waist. (h) Output signals with the elbow bent at 30°, 45°, 60°, 90° and 120°. (i) Output signals in response with knee bending at 30°, 45°, 60°, 90°, and 120°.

constant power to portable electronic devices, the real-time voltage output of the TI-TENG is measured for 2400 s upon contact-separation at a frequency of 2 Hz, which shows a relatively stable output with almost no fluctuations (Fig. S14f). Then the TI-TENG is presented to power an electronic watch (Fig. S14g, Movie S3) and power a temperature and humidity sensor (Fig. S14h, Movie S4) by in-series connecting with a 33 μF capacitor or a 100 μF capacitor, respectively. The inner and outer textile used in the TI-TENG are well packaged with lightness and thinness, which makes them more suitable for the practical needs of long-time outdoor activities than conventional power supplies based on metallic and plastic materials.

Supplementary material related to this article can be found online at doi:10.1016/j.nanoen.2023.109134.

Supplementary material related to this article can be found online at doi:10.1016/j.nanoen.2023.109134.

In addition to working as a power source, the applied force or strain is also closely correlated to the electrical output of the TI-TENG, which allows it to work as a self-powered (bio)mechanical sensor. During its operation, the packaged TI-TENG can directly contact with human skin or other objects, realzing the function of motion monitoring (Fig. 5**a**). The magnitude of the applied static pressure is reflected by using the V_{OC} as the sensing signal of TI-TENG. Fig. 5**b** records the real-time V_{OC} as sensing signal under different pressures, with the signal consistently increasing from 7.03 to 69.71 V as the pressure increases from 0.288 to 14.4 kPa. This result is attributed to that the increased pressure leads to an increase in the deformability of the TI-textiles, resulting in a contact-area increment and enhanced TI-TENG outputs. The ratio between the voltage change and the applied pressure, defined as pressure sensitivity (i.e., $\Delta V/P$), is evaluated into two typical sensory ranges (a high sensitivity range below 2.69 kPa at a sensitivity of 10.76487 V·kPa^{-1}, and a relatively low sensitivity range above 2.69 kPa at a sensitivity of 3.39209 V·kPa^{-1}) (Fig. 5**c**). The normalized sensitivity ($(V\text{-}V_0)/V_0$) in the high and low sensitivity regions is 1.53346 and 0.4832 kPa^{-1}, respectively (Fig. S15a). The initial contact process at lower pressures (<2.69 kPa) will result in a relatively large deformation of the TI-TENG, while the later compression process at higher pressures (>2.69 kPa) will result in a comparatively small deformation. This is because the deformation space of the TI-TENG sensor is reduced in the high-pressure range. A detailed comparison of the sensitivities in this work with several relevant studies is presented in Table S6 [50,60–67]. Based on the high-efficiency contact-separation process caused by the applied external strain, the TI-TENG can work as both pressure sensor and strain sensor. The increased external strain will result in the larger contact area between the TI-textile and the FEP, and lead to the proportionally increasing output sensing signal. To visually represent the stress allocation during the bending-releasing cycle, the TI-TENG deformation at a bending angle of 60° is simulated by COMSOL Multiphysics (Fig. S15b and S15c) [68]. As the TI-TENG is cyclically bent and released (Fig. S15d), the real-time voltage outputs show a simultaneous increase/decrease as a result of the electron transfer process between the TI-textile and FEP layer. It is remarkable that as the bending angle increases from 30° to 90°, the output voltage signal of the TI-TENG increases from 28.70 to 52.64 V, indicating a good linearity between the output signal vs. bending angle ($R^2 = 0.998$).

During the daily life or outdoor activities, different human motions have dissimilar physiological characteristics and can be reflected by the different bending/stretching of the human joints. The articular flexion data can also be of great assistance in the medical convalescence and outdoor activity recording (or rescue). According to the flexibility, versatility, high sensitivity of the TI-TENG mechanical sensor, it can be readily attached to different human joints assisted with fabric-woven belts for action recognition, medical detection, and outdoor rescue in a self-powered, fast-responsive, and real-time means. To monitor different human motions, the TI-TENG can be worn on the shoulders, wrists, elbows, waist, hips, and knees (the most common areas of the paralyzed patient's body for recovery) or worn on the hips and knees (body joints that indicate abnormalities in outdoor falling). It is notable that the shape retention and contact improvement of the TI-TENG with human skin have a positive and significant impact on the sensing performances. As demonstrated in Fig. 5**d**, the periodic shoulder swing leads to periodically electrical sensing signals. There will be a smaller output sensing signal upon smaller bending angle (load force is also small in this case) [69]. When the volunteer swings the arm from 0° to 120°, the TI-TENG at the shoulder is exposed to an increased load force, which leads to a larger contact area of the frication layer and raises the TI-TENG output sensing performance. By fixing the TI-TENG on the wrist, the variations of voltage signal can also be easily monitored at the bend-release cycles (bending angles from 30° to 90°, Fig. 5**e**). By wearing the TI-TENG at the hip and waist, it is even possible to distinguish the hip being driven up/down by the leg (Fig. 5**f**) and the waist twisting from side to side (Fig. 5**g**). For elbow monitoring, it may be possible for patients with elbow injuries to recover upper limb movements and control their own movements through monitoring/training, which may also facilitate remote human-machine interaction and supervision. When the TI-TENG strain sensor is worn on the elbow, it can record the real-time flexion/extension of the arm to different angles with periodic voltage signals (Fig. 5**h**). In addition to above discussed body joints, human leg is the primary body recovery position to be monitored, which can help assess the recovery status of the paralyzed patients and facilitate automatic alarms in the accident of a fall and shortens the rescue time. Corresponding sensing signals under various bending angles are monitored as shown in Fig. 5**i**. According to these electrical signals, corresponding body movements can be recorded for healthcare rehabilitation or outdoor rescue.

Generally, the constant absorption and emission of Infrared Rays (IR) from the body into the environment is the primary cause of thermal loss. Especially in the case of severe weather extremes, the heat requirements of the human body for long-time outdoor motion can be effectively provided. In addition to the demonstration as sweat sensors, energy harvesters, and biomechanical sensors, the reported TI-TENG can also significantly keep warm by preventing the loss of radiant heat from the body. To evaluate the radiation isolation capabilities of the TI-TENG (i.e., the TI-textile packaged with outer windproof textile and inner lining textile), we take the same method with the previous characterization means. As shown in Fig. S16b, three different samples (only TI-textile, only inner and outer textile, and TI-textile packaged with inner and outer textile) are characterized on a hot plate in ambient environment. First of all, the hot plate is set at a temperature of 65 °C. The samples are placed on the hot plate and their temperature variations are monitored in real time using the digital thermometer (Fig. S16a). The temperature drop ΔT for only TI-textile, only inner and outer textile, and the packaged TI-textile are 7 °C, 5.5 °C, and 7.7 °C, respectively. As ΔT is proportional to the thermal insulating properties, the performance of packaged TI-textile is the best compared with other two samples. In addition, the temperatures of the hot plate are also set to 45 °C, 75 °C, and 54 °C (Fig. S16c-S16e) to obtain the tendency of temperature drops for the three samples (also concluded in Table S5). Thermal images from infrared camera of the three samples placed on the palm (Fig. S16b, after thermal equilibrium) also vividly demonstrate the best thermal insulating properties of packaged TI-textile. The measured average temperatures for only TI-textile, only inner and outer textile, and packaged TI-textile are 31.5 °C, 31.8 °C, and 28.5 °C, respectively. All the above results verify that the packaged TI-textile (consistent with the structure of TI-TENG) has the best thermal insulating performances and it can be readily applied to outdoor clothes for long-time excises or outdoor activities.

For some extreme outdoor activities, once there is an accident, it will be very difficult to call for help quickly and the probability of injuries or deaths may increase in a complex and ever-changing environment [70]. If the conventional battery-powered sensors suddenly stop operating, people may face more difficulties in seeking for rescue. Based on the versatile TI-TENG, we have also developed a multifunctional outdoor

rescue system by using the TI-TENG as a self-powered wireless signal-transmission sensor for human-machine interactive interface. Fig. 6**a** schematically presents the operating process of the outdoor rescue system, which consists of a TI-TENG-based dressing belt, a Global System for Mobile Communications (GSM) module, a signal processing circuit, and a card for the mobile phone. During operation, the TI-TENG-based dressing belt allows continuous real-time monitoring on the body's respiratory status, and it can also be taken on the hip and knee to monitor relevant movement. The signal treatment circuit consists of a signal amplification function (magnify the electrical signal and remove unwanted interference), a voltage comparator (transform the amplified signal into the stabilized square wave signal), and an Arduino board (receive the square wave signals and send trigger commands to the GSM). For instance, when some abnormal falling signals are monitored by TI-TENG worn on the hip or knee (Fig. 6**b**), one can press/touch the trigger TI-TENG and send instructions to the Arduino board, which can activate the GSM module and call for help (Fig. 6**c** and Movie S5, two TI-TENGs in single electrode mode are connected to the two channels of save our souls (SOS) which are "Emergency contact" and "Family contact", respectively). In addition to outdoor rescue, the TI-TENG can also be used as an interactive interface for some entertainments (e.g., touch to play music) during the outdoor activities or long journeys. Fig. 6**d** schematically illustrates the TI-TENG based interactive music player. When the finger touches the TI-TENG, the triggered signal (over threshold, Fig. 6**e**) can readily control the Raspberry Pi and send a wireless signal to play music via Bluetooth module. The keys in the music player ("Play", "Pause", "Next", "Previous") are realized by using different TI-TENG sensors connected to different channels and their signals can be independently recognized (Fig. 6**f**) [49,71]. The monitored real-time trigger signals and the music controlling process (e.g., "Play/Pause", "Previous song", "Next song") are shown in Fig. S17 and Movie S6.

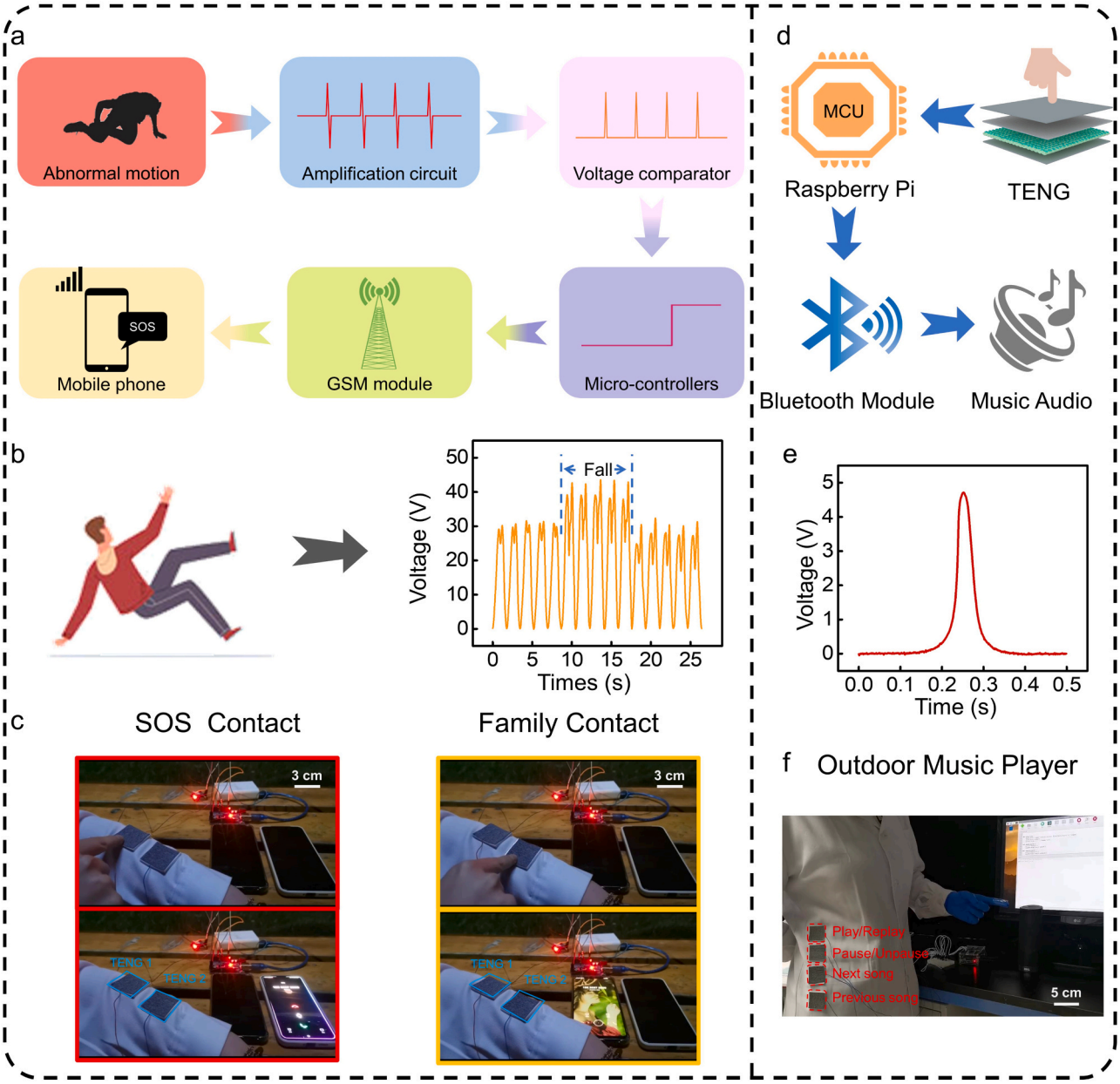

Fig. 6. Demonstration of the outdoor interactive applications. (a) Schematic illustration of a real-time safety surveillance and smart outdoor rescue system. (b) Electrical signal generated under an accidental fall. (c) Photographs of a personal outdoor rescue system in practical application. (d) Wireless music playing system by TI-TENG. (e) An electrical signal output on finger touch. (f) The outdoor music player triggered by the finger via the TI-TENG.

Supplementary material related to this article can be found online at doi:10.1016/j.nanoen.2023.109134.

Supplementary material related to this article can be found online at doi:10.1016/j.nanoen.2023.109134.

3. Conclusion

In summary, a multi-layer TI-TENG packaged with the inner and outer textiles is designed and manufactured into a self-powered sensory and interactive system for outdoor activities, exhibiting the advantages of excellent flexibility, high thermal insulating properties, high antibacterial activities, lightweight, and quick drying performance compared with previously reported textile TENGs (Table S7). We have also optimized the materials, the number of layers, and the structures to improve the performances of TI-TENG utilizing it to harvest biomechanical energy in outdoors. Thanks to the superior thermal insulating performance of the TI-textile, the thermal management during outdoor activities is also available to be achieved. The demonstrated multifunctional sensors and human-machine interactive system based on the TI-TENG can be readily used for motion detection, health monitoring, and wireless transmission. The available large-scale production of multilayer thermal insulating textiles for multifunctional sensors opens a new way to the development of outdoor electronics and flexible wearable devices in future.

4. Experiments

4.1. Fabrication of TI-TENG and the packaged TI-TENG

For the systematic design of the TI-TENG, commercial TI-textile (thickness: 0.27 mm, Beijing Matrix Technologies Co., Ltd.) and FEP are selected as the triboelectric materials, silver tape is chosen as the outer electrode, and the windproof textile and textile lining are selected as the packing textile (area of 3 × 3 cm^2). At the same time, TI-TENG lacks the windproof textile (outer layer) and textile lining (inner layer) compared to the packaged TI-TENG. Also, an Ag-coated Nylon with flexibility is chosen for the electrodes. A non-conductive cotton string is used to hold them together.

4.2. Electrical output measurement

To measure the output performance of the TI-TENG and the packaged TI-TENG, the action of contact-separation is driven by a numerically-controlled linear motor. Triboelectric outputs (I_{SC}, V_{OC}, and Q_{SC}) are tested by using Keithley 6514. A customized LabVIEW program is employed to record the electrical outputs. The current signals generated by the TI-TENG for real-time recognition are collected by the Keithley 6514 Electrometer. The electrical potential between the FEP and TI-textile is simulated by employing the finite element method using the commercially available COMSOL Multiphysics. The finite element simulation method is also employed for the bending condition of the TI-TENG.

Regarding to output performances in relation to external load, the output signals according to different load resistances are tested in parallel with a Keithley 6514 electrometer. The power density corresponding to external load is calculated according to $P = \frac{V^2}{R}$, where R, V, P are the resistance of the external load, the output voltage, and the peak power, respectively. The average power density is calculated according to $P_{ave} = \frac{\int_0^T U^2 dt}{RTS}$. The outputs of different capacitors are also measured by the Keithley 6514, which is in parallel connected when the capacitors are charged.

For the pressure sensor, the external force is applied by a linear mechanical motor. The applied force is sensed by a force detector (YMC 501F01, 8 mm diameter) monitored by an oscilloscope. Keithley 6514 is also used to check the voltage in relation to the stress situation. The air permeability of TENG is tested by YG461E air permeability tester, and the testing standard is GB_T5453:1997.

4.3. The fabrication of sweat sensors

Sixteen pieces of TI-textile are cut into square area in 3 cm × 3 cm. Subsequently, NaCl powder corresponding to the mass of different concentrations of NaCl solution (0.001–1 mol/L) is weighted with an electronic balance. The weighted NaCl powder is dissolved in 20 ml of DI water and stirred until it is completely dissolved. Afterwards, the TI-textiles are put into different concentrations of NaCl solution as well as DI water, respectively, and left to stand at room temperature for 2 h until the liquid completely immerses the TI-textiles. After that, sixteen pieces of TI-textiles are dried in an oven at 35 °C (close to the temperature of body temperature) for 2 h. Finally, TI-textiles immersed in different concentrations of NaCl solution are assembled into TI-TENGs.

Author statement

This manuscript has not been published or presented elsewhere in part or in entirety, and is not under consideration by another journal. All the authors have approved the manuscript and agree with submission to your esteemed journal. There are no conflicts of interest to declare.

Declaration of Competing Interest

The authors declare that they have no known competing financial interests or personal relationships that could have appeared to influence the work reported in this paper.

Data availability

Data will be made available on request.

Acknowledgements

This work is financially supported by the National Key Research and Development Program of China (2021YFB3200304), the National Natural Science Foundation of China (52073031, 22008151), Beijing Nova Program (Z211100002121148), and the “Hundred Talents Program” of the Chinese Academy of Sciences.

Appendix A. Supporting information

Supplementary data associated with this article can be found in the online version at doi:10.1016/j.nanoen.2023.109134.

References

[1] Z.L. Wang, A.C. Wang, On the origin of contact-electrification, Mater. Today 30 (2019) 34–51.
[2] T. Kim, S. Jeon, S. Lone, S.J. Doh, D.M. Shin, H.K. Kim, Y.H. Hwang, S.W. Hong, Versatile nanodot-patterned Gore-Tex fabric for multiple energy harvesting in wearable and aerodynamic nanogenerators, Nano Energy 54 (2018) 209–217.
[3] Y.Y. Luo, Y.Z. Li, P. Sharma, W. Shou, K. Wu, M. Foshey, B.C. Li, T. Palacios, A. Torralba, W. Matusik, Learning human-environment interactions using conformal tactile textiles (vol 4, pg 193, 2021), Nat. Electron. 4 (4) (2021), 314-314.
[4] K. Bayoumy, M. Gaber, A. Elshafeey, O. Mhaimeed, E.H. Dineen, F.A. Marvel, S. S. Martin, E.D. Muse, M.P. Turakhia, K.G. Tarakji, M.B. Elshazly, Smart wearable devices in cardiovascular care: where we are and how to move forward, Nat. Rev. Cardiol. 18 (8) (2021) 581–599.
[5] K. Dong, Y. Hu, J. Yang, S.-W. Kim, W. Hu, Z.L. Wang, Smart textile triboelectric nanogenerators: Current status and perspectives, MRS Bull. 46 (6) (2021) 512–521.
[6] F.-R. Fan, Z.-Q. Tian, Z. Lin Wang, Flexible triboelectric generator, Nano Energy 1 (2) (2012) 328–334.
[7] Z.L. Wang, Triboelectric nanogenerators as new energy technology for self-powered systems and as active mechanical and chemical sensors, Acs Nano 7 (11) (2013) 9533–9557.

[8] S. Niu, X. Wang, F. Yi, Y.S. Zhou, Z.L. Wang, A universal self-charging system driven by random biomechanical energy for sustainable operation of mobile electronics, Nat. Commun. 6 (2015) 8975.

[9] Z.L. Wang, J. Chen, L. Lin, Progress in triboelectric nanogenerators as a new energy technology and self-powered sensors, Energy Environ. Sci. 8 (8) (2015) 2250–2282.

[10] J.M. Chen, K.E. Schutz, C.B. Tucker, Sprinkler flow rate affects dairy cattle preferences, heat load, and insect deterrence behavior, Appl. Anim. Behav. Sci. 182 (2016) 1–8.

[11] D. Choo, S. Yang, C. Lee, W. Kim, J. Kim, J. Hong, Highly surface-embossed polydimethylsiloxane-based triboelectric nanogenerators with hierarchically nanostructured conductive Ni-Cu fabrics, Acs Appl. Mater. Inter 10 (39) (2018) 33221–33229.

[12] Z.L. Li, J.L. Shen, I. Abdalla, J.Y. Yu, B. Ding, Nanofibrous membrane constructed wearable triboelectric nanogenerator for high performance biomechanical energy harvesting, Nano Energy 36 (2017) 341–348.

[13] M. Wang, N. Zhang, Y.J. Tang, H. Zhang, C. Ning, L. Tian, W.H. Li, J.H. Zhang, Y. C. Mao, E.J. Liang, Single-electrode triboelectric nanogenerators based on sponge-like porous PTFE thin films for mechanical energy harvesting and self-powered electronics, J. Mater. Chem. A 5 (24) (2017) 12252–12257.

[14] H. Zou, L. Guo, H. Xue, Y. Zhang, X. Shen, X. Liu, P. Wang, X. He, G. Dai, P. Jiang, H. Zheng, B. Zhang, C. Xu, Z.L. Wang, Quantifying and understanding the triboelectric series of inorganic non-metallic materials, Nat. Commun. 11 (1) (2020), 2093.

[15] H. Zou, Y. Zhang, L. Guo, P. Wang, X. He, G. Dai, H. Zheng, C. Chen, A.C. Wang, C. Xu, Z.L. Wang, Quantifying the triboelectric series, Nat. Commun. 10 (1) (2019), 1427.

[16] D.H. Kim, B. Dudem, J.S. Yu, High-performance flexible piezoelectric-assisted triboelectric hybrid nanogenerator via polydimethylsiloxane-encapsulated nanoflower-like ZnO composite films for scavenging energy from daily human activities, ACS Sustain. Chem. Eng. 6 (7) (2018) 8525–8535.

[17] Z.L. Li, M.M. Zhu, Q. Qiu, J.Y. Yu, B. Ding, Multilayered fiber-based triboelectric nanogenerator with high performance for biomechanical energy harvesting, Nano Energy 53 (2018) 726–733.

[18] Y.T. Qian, D.J. Kangg, Poly(dimethylsiloxane)/ZnO Nanoflakes/three-dimensional graphene heterostructures for high-performance flexible energy harvesters with simultaneous piezoelectric and triboelectric generation, ACS Appl. Mater. Inter 10 (38) (2018) 32281–32288.

[19] S.Y. Shin, B. Saravanakumar, A. Ramadoss, S.J. Kim, Fabrication of PDMS-based triboelectric nanogenerator for self-sustained power source application, Int J. Energ. Res 40 (3) (2016) 288–297.

[20] Q.K. Ye, Y.Z. Wu, Y.Y. Qi, L. Shi, S.Y. Huang, L. Zhang, M.L. Li, W. Li, X.Y. Zeng, H. L. Wo, X.Z. Wang, S.R. Dong, S. Ramakrishna, J.K. Luo, Effects of liquid metal particles on performance of triboelectric nanogenerator with electrospun polyacrylonitrile fiber films, Nano Energy 61 (2019) 381–388.

[21] D.L. Li, C.X. Wu, L. Ruan, J.X. Wang, Z.R. Qiu, K. Wang, Y. Liu, Y.F. Zhang, T. L. Guo, J.T. Lin, T.W. Kim, Electron-transfer mechanisms for confirmation of contact-electrification in ZnO/polyimide-based triboelectric nanogenerators, Nano Energy 75 (2020) 2211–2855.

[22] X. Pu, J.W. Zha, C.L. Zhao, S.B. Gong, J.F. Gao, R.K.Y. Li, Flexible PVDF/nylon-11 electrospun fibrous membranes with aligned ZnO nanowires as potential triboelectric nanogenerators, Chem. Eng. J. 398 (2020) 1385–8947.

[23] W. He, Y. Qian, B.S. Lee, F. Zhang, A. Rasheed, J.E. Jung, D.J. Kang, Ultrahigh output piezoelectric and triboelectric hybrid nanogenerators based on ZnO nanoflakes/polydimethylsiloxane composite films, ACS Appl. Mater. Interfaces 10 (51) (2018) 44415–44420.

[24] L.Y. Lan, C.M. Jiang, Y. Yao, J.F. Ping, Y.B. Ying, A stretchable and conductive fiber for multifunctional sensing and energy harvesting, Nano Energy 84 (2021) 2211–2855.

[25] Z. Qin, Y.Y. Yin, W.Z. Zhang, C.J. Li, K. Pan, Wearable and stretchable triboelectric nanogenerator based on crumpled nanofibrous membranes, Acs Appl. Mater. Inter 11 (13) (2019) 12452–12459.

[26] L.Y. Lan, J.Q. Xiong, D.C. Gao, Y. Li, J. Chen, J. Lv, J.F. Ping, Y.B. Ying, P.S. Lee, Breathable nanogenerators for an on-plant self-powered sustainable agriculture system, ACS Nano 15 (3) (2021) 5307–5315.

[27] G.L. Ni, X.S. Zhu, H.Y. Mi, P.Y. Feng, J. Li, X. Jing, B.B. Dong, C.T. Liu, C.Y. Shen, Skinless porous films generated by supercritical CO_2 foaming for high-performance complementary shaped triboelectric nanogenerators and self-powered sensors, Nano Energy 87 (2021) 2211–2855.

[28] J. Han, C.Y. Xu, J.T. Zhang, N. Xu, Y. Xiong, X.L. Cao, Y.C. Liang, L. Zheng, J. Sun, J.Y. Zhai, Q.J. Sun, Z.L. Wang, Multifunctional coaxial energy fiber toward energy harvesting, storage, and utilization, ACS Nano 15 (1) (2021) 1597–1607.

[29] S.M. Hu, J. Han, Z.J. Shi, K. Chen, N. Xu, Y.F. Wang, R.Z. Zheng, Y.Z. Tao, Q.J. Sun, Z.L. Wang, G. Yang, Biodegradable, super-strong, and conductive cellulose macrofibers for fabric-based triboelectric nanogenerator, Nano-Micro Lett. 14 (1) (2022), 115.

[30] Y. Xiong, L. Luo, J.H. Yang, J. Han, Y. Liu, H.S. Jiao, S.S. Wu, L.Q. Cheng, Z. Y. Feng, J. Sun, Z.L. Wang, Q.J. Sun, Scalable spinning, winding, and knitting graphene textile TENG for energy harvesting and human motion recognition, Nano Energy 107 (2023) 2211–2855.

[31] J. Zhuo, Z. Zheng, R. Ma, X. Zhang, Y. Wang, P. Yang, L. Cao, J. Chen, J. Lu, G. Chen, G. Chen, J. Fu, Z. Wu, J. Wang, X. Wang, G. Yang, F. Yi, A breathable and woven hybrid energy harvester with optimized power management for sustainably powering electronics, Nano Energy 112 (2023), 108436.

[32] C. Wei, R. Cheng, C. Ning, X. Wei, X. Peng, T. Lv, F. Sheng, K. Dong, Z.L. Wang, A self-powered body motion sensing network integrated with multiple triboelectric fabrics for biometric gait recognition and auxiliary rehabilitation training, Adv. Funct. Mater. 33 (35) (2023), 2303562.

[33] Y. Cheng, J. Wang, X. Lu, C. Wang, An all-nanofibrous Janus textile with directional perspiration for triboelectric nanogenerator and self-powered e-skin sensor, Nano Energy 117 (2023), 108852.

[34] Y. Gao, B. Xu, D. Tan, M. Li, Y. Wang, Y. Yang, Asymmetric-elastic-structure fabric-based triboelectric nanogenerators for wearable energy harvesting and human motion sensing, Chem. Eng. J. 466 (2023), 143079.

[35] L. Feng, S. Xu, T. Sun, C. Zhang, J. Feng, L. Yao, J. Ge, Fire/acid/alkali-resistant aramid/carbon nanofiber triboelectric nanogenerator for self-powered biomotion and risk perception in fire and chemical environments, Adv. Fiber Mater. 5 (4) (2023) 1478–1492.

[36] X. Zhong, T. Song, H. Dong, S. Jiang, R. Wei, Ionogel based triboelectric nanogenerator textiles for high-precision human fall recognition, Chem. Eng. J. 474 (2023), 145686.

[37] M. Cheng, X. Liu, Z. Li, Y. Zhao, X. Miao, H. Yang, T. Jiang, A. Yu, J. Zhai, Multiple textile triboelectric nanogenerators based on UV-protective, radiative cooling, and antibacterial composite yarns, Chem. Eng. J. 468 (2023), 143800.

[38] C. Fan, Z. Long, Y. Zhang, A. Mensah, H. He, Q. Wei, P. Lv, Robust integration of energy harvesting with daytime radiative cooling enables wearing thermal comfort self-powered electronic devices, Nano Energy 116 (2023), 108842.

[39] D. Doganay, O. Demircioglu, M. Cugunlular, M.O. Cicek, O. Cakir, H.U. Kayaci, S. Ç. Aygün, H.E. Unalan, Wet spun core-shell fibers for wearable triboelectric nanogenerators, Nano Energy 116 (2023), 108823.

[40] L. Shang, Z. Wu, X. Li, A. Xu, Y. Miao, W. Xu, W. Tang, C. Fu, B. Su, K. Dong, Z. Xia, A breathable and highly impact-resistant shear-thickened fluid (STF) based TENG via hierarchical liquid-flow spinning for intelligent protection, Nano Energy 118 (2023), 108955.

[41] K.Y. Meng, S.L. Zhao, Y.H. Zhou, Y.F. Wu, S.L. Zhang, Q. He, X. Wang, Z.H. Zhou, W.J. Fan, X.L. Tan, J. Yang, J. Chen, A wireless textile-based sensor system for self-powered personalized health care, Matter 2 (4) (2020) 896–907.

[42] Z.H. Zhou, K. Chen, X.S. Li, S.L. Zhang, Y.F. Wu, Y.H. Zhou, K.Y. Meng, C.C. Sun, Q. He, W.J. Fan, E.D. Fan, Z.W. Lin, X.L. Tan, W.L. Deng, J. Yang, J. Chen, Sign-to-speech translation using machine-learning-assisted stretchable sensor arrays, Nat. Electron. 3 (9) (2020) 571–578.

[43] Z.H. Zhou, L. Weng, T. Tat, A. Libanori, Z.M. Lin, L.J. Ge, J. Yang, J. Chen, Smart insole for robust wearable biomechanical energy harvesting in harsh environments, ACS Nano 14 (10) (2020) 14126–14133.

[44] Z.W. Lin, G.Q. Zhang, X. Xiao, C. Au, Y.H. Zhou, C.C. Sun, Z.H. Zhou, R. Yan, E. D. Fan, S.B. Si, L. Weng, S. Mathur, J. Yang, J. Chen, A personalized acoustic interface for wearable human-machine interaction, Adv. Funct. Mater. 32 (9) (2022), 2109430.

[45] P.C. Hsu, X. Liu, C. Liu, X. Xie, H.R. Lee, A.J. Welch, T. Zhao, Y. Cui, Personal thermal management by metallic nanowire-coated textile, Nano Lett. 15 (1) (2015) 365–371.

[46] Q. Liu, J. Huang, J. Zhang, Y. Hong, Y. Wan, Q. Wang, M. Gong, Z. Wu, C.F. Guo, Thermal, waterproof, breathable, and antibacterial cloth with a nanoporous structure, ACS Appl. Mater. Interfaces 10 (2) (2018) 2026–2032.

[47] Y. Guo, K. Li, C. Hou, Y. Li, Q. Zhang, H. Wang, Fluoroalkylsilane-modified textile-based personal energy management device for multifunctional wearable applications, ACS Appl. Mater. Interfaces 8 (7) (2016) 4676–4683.

[48] Y.-T. Jao, P.-K. Yang, C.-M. Chiu, Y.-J. Lin, S.-W. Chen, D. Choi, Z.-H. Lin, A textile-based triboelectric nanogenerator with humidity-resistant output characteristic and its applications in self-powered healthcare sensors, Nano Energy 50 (2018) 513–520.

[49] Y. Yang, J. Han, J. Huang, J. Sun, Z.L. Wang, S. Seo, Q. Sun, Stretchable energy-harvesting tactile interactive interface with liquid-metal-nanoparticle-based electrodes, Adv. Funct. Mater. 30 (29) (2020), 1909652.

[50] J. Han, C. Xu, J. Zhang, N. Xu, Y. Xiong, X. Cao, Y. Liang, L. Zheng, J. Sun, J. Zhai, Q. Sun, Z.L. Wang, Multifunctional coaxial energy fiber toward energy harvesting, storage, and utilization, ACS Nano 15 (1) (2021) 1597–1607.

[51] S. Niu, S. Wang, L. Lin, Y. Liu, Y.S. Zhou, Y. Hu, Z.L. Wang, Theoretical study of contact-mode triboelectric nanogenerators as an effective power source, Energy Environ. Sci. 6 (12) (2013) 3576.

[52] N. Zheng, J. Xue, Y. Jie, X. Cao, Z.L. Wang, Wearable and humidity-resistant biomaterials-based triboelectric nanogenerator for high entropy energy harvesting and self-powered sensing, Nano Res. 15 (7) (2022) 6213–6219.

[53] Q. Lu, H. Chen, Y. Zeng, J. Xue, X. Cao, N. Wang, Z. Wang, Intelligent facemask based on triboelectric nanogenerator for respiratory monitoring, Nano Energy 91 (2022), 106612.

[54] K. Dong, X. Peng, J. An, A.C. Wang, J. Luo, B. Sun, J. Wang, Z.L. Wang, Shape adaptable and highly resilient 3D braided triboelectric nanogenerators as e-textiles for power and sensing, Nat. Commun. 11 (1) (2020), 2868.

[55] Z.L. Wang, On the first principle theory of nanogenerators from Maxwell's equations, Nano Energy 68 (2020), 104272.

[56] D. Choi, H. Lee, D.J. Im, I.S. Kang, G. Lim, D.S. Kim, K.H. Kang, Spontaneous electrical charging of droplets by conventional pipetting, Sci. Rep. 3 (2013) 2037.

[57] K. Yatsuzuka, Y. Higashiyama, K. Asano, Electrification of polymer surface caused by sliding ultrapure water, Ieee T Ind. Appl. 32 (4) (1996) 825–831.

[58] S.-B. Jeon, M.-L. Seol, D. Kim, S.-J. Park, Y.-K. Choi, Self-powered ion concentration sensor with triboelectricity from liquid-solid contact electrification, Adv. Electron. Mater. 2 (5) (2016), 1600006.

[59] J. Nie, Z. Ren, L. Xu, S. Lin, F. Zhan, X. Chen, Z.L. Wang, Probing contact-electrification-induced electron and ion transfers at a liquid-solid interface, Adv. Mater. 32 (2) (2020), e1905696.

[60] Z. Li, M. Zhu, J. Shen, Q. Qiu, J. Yu, B. Ding, All-fiber structured electronic skin with high elasticity and breathability, Adv. Funct. Mater. 30 (6) (2019), 1908411.
[61] X. Peng, K. Dong, C. Ning, R. Cheng, J. Yi, Y. Zhang, F. Sheng, Z. Wu, Z.L. Wang, All-nanofiber self-powered skin-interfaced real-time respiratory monitoring system for obstructive sleep apnea-hypopnea syndrome diagnosing, Adv. Funct. Mater. 31 (34) (2021), 2103559.
[62] X. Peng, K. Dong, C. Ye, Y. Jiang, S. Zhai, R. Cheng, D. Liu, X. Gao, J. Wang, Z. L. Wang, A breathable, biodegradable, antibacterial, and self-powered electronic skin based on all-nanofiber triboelectric nanogenerators, Sci. Adv. 6 (26) (2020), eaba9624.
[63] X. Guan, B. Xu, M. Wu, T. Jing, Y. Yang, Y. Gao, Breathable, washable and wearable woven-structured triboelectric nanogenerators utilizing electrospun nanofibers for biomechanical energy harvesting and self-powered sensing, Nano Energy 80 (2021), 105549.
[64] P. Yang, Y. Shi, S. Li, X. Tao, Z. Liu, X. Wang, Z.L. Wang, X. Chen, Monitoring the degree of comfort of shoes in-motion using triboelectric pressure sensors with an ultrawide detection range, ACS Nano 16 (3) (2022) 4654–4665.
[65] Q.-J. Sun, Y. Lei, X.-H. Zhao, J. Han, R. Cao, J. Zhang, W. Wu, H. Heidari, W.-J. Li, Q. Sun, V.A.L. Roy, Scalable fabrication of hierarchically structured graphite/polydimethylsiloxane composite films for large-area triboelectric nanogenerators and self-powered tactile sensing, Nano Energy 80 (2021), 105521.
[66] J. Yu, X. Hou, J. He, M. Cui, C. Wang, W. Geng, J. Mu, B. Han, X. Chou, Ultra-flexible and high-sensitive triboelectric nanogenerator as electronic skin for self-powered human physiological signal monitoring, Nano Energy 69 (2020), 104437.
[67] X. Pu, M.M. Liu, X.Y. Chen, J.M. Sun, C.H. Du, Y. Zhang, J.Y. Zhai, W.G. Hu, Z. L. Wang, Ultrastretchable, transparent triboelectric nanogenerator as electronic skin for biomechanical energy harvesting and tactile sensing, Sci. Adv. 3 (5) (2017), e1700015.
[68] Y. Luo, Z. Wang, J. Wang, X. Xiao, Q. Li, W. Ding, H.Y. Fu, Triboelectric bending sensor based smart glove towards intuitive multi-dimensional human-machine interfaces, Nano Energy 89 (2021), 106330.
[69] M. He, W. Du, Y. Feng, S. Li, W. Wang, X. Zhang, A. Yu, L. Wan, J. Zhai, Flexible and stretchable triboelectric nanogenerator fabric for biomechanical energy harvesting and self-powered dual-mode human motion monitoring, Nano Energy 86 (2021), 106058.
[70] L. Niu, X. Peng, L. Chen, Q. Liu, T. Wang, K. Dong, H. Pan, H. Cong, G. Liu, G. Jiang, C. Chen, P. Ma, Industrial production of bionic scales knitting fabric-based triboelectric nanogenerator for outdoor rescue and human protection, Nano Energy 97 (2022), 107168.
[71] J. Zhang, S. Hu, Z. Shi, Y. Wang, Y. Lei, J. Han, Y. Xiong, J. Sun, L. Zheng, Q. Sun, G. Yang, Z.L. Wang, Eco-friendly and recyclable all cellulose triboelectric nanogenerator and self-powered interactive interface, Nano Energy 89 (2021), 106354.